Geochemistry Geophysics Geosystems G3
AN ELECTRONIC JOURNAL OF THE EARTH SCIENCES
Published by AGU and the Geochemical Society

Article
Volume 6, Number 5
5 May 2005
Q05004, doi:10.1029/2004GC000751
ISSN: 1525-2027

Localized versus distributed shear in transform plate boundary zones: The case of the Dead Sea Transform in the Jericho Valley

G. Shamir
Geophysical Institute of Israel, P.O. Box 182, Lod 71100, Israel (gadi@seis.mni.gov.il)

Y. Eyal
Geology Department, Ben Gurion University, Beer-Sheva, Israel (eyal@bgumail.bgu.ac.il)

I. Bruner
Ecolog Engineering Ltd., 5/44 Oppenheimer Street, Rehovot, Israel (bruneri@ecolog.co.il)

[1] Continental transform plate boundaries are typically either localized along a single, usually segmented, major fault or distributed over a broad deformation zone. In the latter, shear is partitioned between major strike slip faults and intervening, often rotating, fault systems. Analog and numerical simulations suggest that such internal fault systems evolve and may be localized or delocalized depending on strain and fault zone strength. This paper examines the degree and evolution of shear localization in the Jericho Valley section of the Dead Sea Transform (DST), which is part of the Africa/Arabia plate boundary. In this section, the current breadth of the transform valley and its penetrative strain field are difficult to reconcile with localized shear. We integrate newly acquired high-resolution reflection data, reprocessed exploration reflection data (both focused to 2.5–3.5 km depth), relatively relocated earthquake epicenters, and fault plane solutions based on P wave first arrivals and suggest reinterpretations for previously published structural and seismic data in the Jericho Valley and the northern Dead Sea basin. It is found that shear in this section of the DST evolved from an early, probably Miocene-Pliocene, stage of localized strike slip motion primarily along the Jericho fault to a late stage (Pliocene-Recent) when shear has been distributed over internal fault sets that apparently lean against a major eastern DST segment. In the early stage the Jericho fault formed the western boundary of a deep, narrow, probably pull-apart basin filled by fluvial clastics and evaporites. This is overlain by the late stage broad basin, characterized by low-energy deposition of lacustrine and fluvial sediments. Pliocene rock salt has apparently utilized the Jericho fault zone as a conduit for diapirism, causing the uplift, normal faulting, and surface deformation of Late Pleistocene and Holocene sediments currently observed along the ~15 km long Jericho Lineament. On the basis of the currently observed dextral-normal motion across the internal NNE-NE trending fault system, counterclockwise rotation is expected to have occurred within the transform zone. These tectonic and depositional changes were probably associated with onset of transtension across the DST, related to the previously postulated shift of the Africa/Arabia Euler pole of rotation in the Pliocene.

Components: 8477 words, 12 figures, 4 tables.

Keywords: Dead Sea; transform plate boundary.

Index Terms: 7230 Seismology: Seismicity and tectonics (1207, 1217, 1240, 1242); 8123 Tectonophysics: Dynamics: seismotectonics; 8150 Tectonophysics: Plate boundary: general (3040).

Received 2 May 2004; **Revised** 17 January 2005; **Accepted** 24 February 2005; **Published** 5 May 2005.

Shamir, G., Y. Eyal, and I. Bruner (2005), Localized versus distributed shear in transform plate boundary zones: The case of the Dead Sea Transform in the Jericho Valley, *Geochem. Geophys. Geosyst.*, *6*, Q05004, doi:10.1029/2004GC000751.

1. Introduction

[2] Shear along continental transform plate boundaries is generally either localized along narrow, usually segmented, major fault zones, or distributed over broad and complex deformation zones. In the first case, stepwise discontinuities and strike changes commonly produce local irrotational compressive or tensile strains, resulting in uplift (''push-up'') or subsidence (''pull-apart''), respectively. This type of plate boundary is observed along much of the extent of the San Andreas fault [*Wallace*, 1990], the North Anatolian fault between the Karliova triple junction and the Sea of Marmara [*Reilinger et al.*, 2000] and the Dead Sea Transform (DST) in the Gulf of Elat/Aqaba [*Ben-Avraham*, 1985] and in the Jordan Valley-Hula segment. Distributed shear plate boundaries, on the other hand, are a few kilometers to several hundred kilometers wide, and consist of a few major strike slip faults and intervening oblique, often rotating, fault systems. These are observed, for example, in the Marlborough fault system in New Zealand [*Lamb and Bibby*, 1989; *Roberts*, 1995], in the Australia-Indonesia shear zone [*Stevens et al.*, 2002], in the Kettleman Hills and Lost Hills anticlines, San Andreas fault zone [*Miller*, 1998], in the San Andreas–San Jacinto fault system, southern California [*Nicholson et al.*, 1986] and in the Korazim block, Dead Sea Transform [*Heimann and Ron*, 1993]. This classification, however, seems to be transient. Laboratory analogs [e.g., *Freund*, 1974; *Schreurs*, 1994; *Beeler et al.*, 1996] and numerical simulations [e.g., *Morgan and Boettcher*, 1999; *Aharonov and Sparks*, 2002], have shown that fault systems formed at low and high angles within broader shear zones (synthetic and antithetic ''Riedel'' shears, respectively) evolve with progressive strain and may be localized or delocalized depending primarily on fault zone strength. In the Dead Sea Transform, field evidence [*Eyal et al.*, 1981] indicates that a shear along the Gulf of Elat/Aqaba segment (Figure 1), initially distributed across a ~40 km wide zone, became progressively more localized with time, to its current segmented form confined to the Gulf.

[3] The Dead Sea Transform (Figure 1), a segmented transform plate boundary aligned with extensional basins, includes sections where the breadth of the transform valley and structures along its margin [*Garfunkel*, 1981] are not easily reconciled with localized shear. The DST is the 18–20 Myr old boundary between the Africa and Arabia plates [*Eyal et al.*, 1981], connecting the Red Sea spreading center in the south to the Alpine convergence zone between Eurasia and Africa/Arabia in the north. The occurrence of a wide transform valley and the abundance of extensional features along the DST has been explained in terms of a change from pure strike-slip to transtension in the Pliocene (~5 Ma) as a result of an eastward 5° shift of its Eulerian pole of rotation [*Joffe and Garfunkel*, 1987].

[4] The broad (up to ~25 km wide) Jericho Valley (Figure 1) forms the northern part of the ~230 km long gravitational and structural Dead Sea Depression (DSD), the deepest continental basin worldwide (estimated maximum depth of ~10 km [*ten Brink et al.*, 1993, 1999]). It is bounded on the west by the high-relief, normal Western Boundary Faults (WBF) of alternating NNW and NE-NNE strike orientations [*Picard*, 1943; *Bentor and Vroman*, 1960]. This bimodal strike distribution also characterizes local [*Gardosh*, 1987; *Shamir et al.*, 2002] and regional [*Sagi*, 1999] fracture systems, morpholineaments in the Jericho Valley [*Belitzky*, 1996; S. Belitzky, personal communication, 2002] and orientation of collapse sinkholes along the western margins of the Dead Sea basin [*Abelson et al.*, 2003]. Within the Jericho Valley, the ~15 km long geomorphic Jericho Lineament (JL), trending 010°, was mapped [*Quennell*, 1956] as part of a major segment of the DST, delimiting a large pull-apart depression in the Dead Sea basin [*Freund*, 1965; *Neev and Hall*, 1979; *Garfunkel*, 1981] (Figure 1). Although sporadic faulting, tilted layers and fracture zones were observed in Pleistocene layers along the JL [*Begin*, 1973; *Reches and Hoexter*, 1981; Z. Garfunkel, personal communication, 2003], this interpretation is difficult to reconcile with the breadth of the Jericho Valley, its lack of microseismicity and the fact that near surface faulting seems to diminish rather than increase southward, toward the Dead Sea basin (S. Marco, personal communication, 2003). *Rotstein et al.* [1991] interpreted exploration seismic reflection lines in the Jericho valley as showing a major DST segment along the Jericho lineament, following *Quennell*'s [1956] map. However, the proximity of their interpreted fault to seismic line terminations and the limited resolution of these seismic lines render this interpretation questionable.

[5] The stratigraphic sequence exposed along the western margins of the Dead Sea basin consists of Mesozoic, mostly carbonate rocks, whereas rocks as old as Paleozoic and Precambrian are exposed in the more elevated eastern margins. Data concerning the depth of the DSB and the thickness

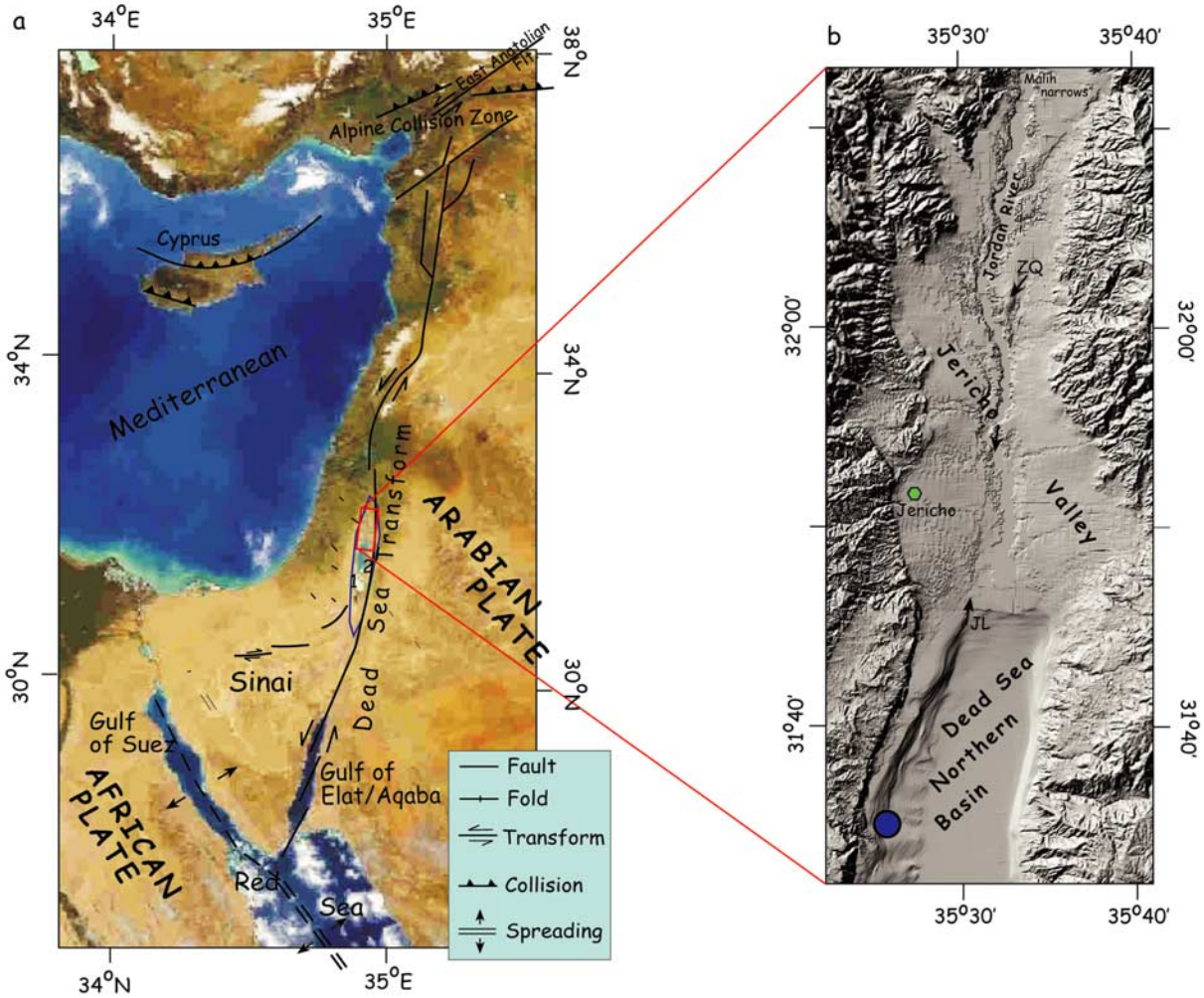

Figure 1. (a) General tectonic setting of the Dead Sea Transform. Blue encircled area, Dead Sea Depression; 1, Mt. Sedom; 2, Lisan Peninsula. (b) The northern Dead Sea Depression. JL, Jericho lineament; ZQ, Zahrat el-Qurein. Full blue circle, epicenter of the $M_L \sim 6.2$ 1927 earthquake [*Shapira et al.*, 1992]. DTM after *Hall* [1993].

of its fill [*Zak*, 1967; *Neev and Emery*, 1967; *Zak and Freund*, 1981; *Kashai and Croker*, 1987] show that the upper Cretaceous, mostly carbonate sequence prevailing west of the DSB is downfaulted into the basin. The basin fill generally includes [*Zak and Freund*, 1981] (1) Middle to Late Miocene, mostly fluvial-clastic terrestrial sand and conglomerates of remote sources (Hatzeva formation). 700–800 m of this formation were recovered in the subsurface in the central DSB; (2) Late Miocene–Pliocene estuarine-lagoonal salt rock, with some marl, anhydrite and shales (Sedom Fm.). This formation produced the large Mt. Sedom and the Lisan diapirs in the central DSB (Figure 1) and probably additional smaller diapirs in the Dead Sea Depression [*Neev and Hall*, 1979; *Belitzky and Mimran*, 1996]. The Sedom formation and its chronostratigraphic equivalents in the northern Jordan Valley were deposited as a result of the Pliocene transgression of the Mediterranean into the DST Valley [*Zak*, 1967]; (3) Pliocene-Holocene lacustrine-fluvial carbonates, evaporites and clastics of local sources (Amora, Samra and Lisan Fms.)

[6] In this study we use new and reprocessed seismic reflection data, relocated earthquake epicenters and calculated fault plane solutions and reinterpretation of previously published structural data to analyze the fault and basin structure in the Jericho Valley section of the DST. It is suggested that plate motion across this section of the plate boundary has evolved from localized to distributed shear, apparently in association

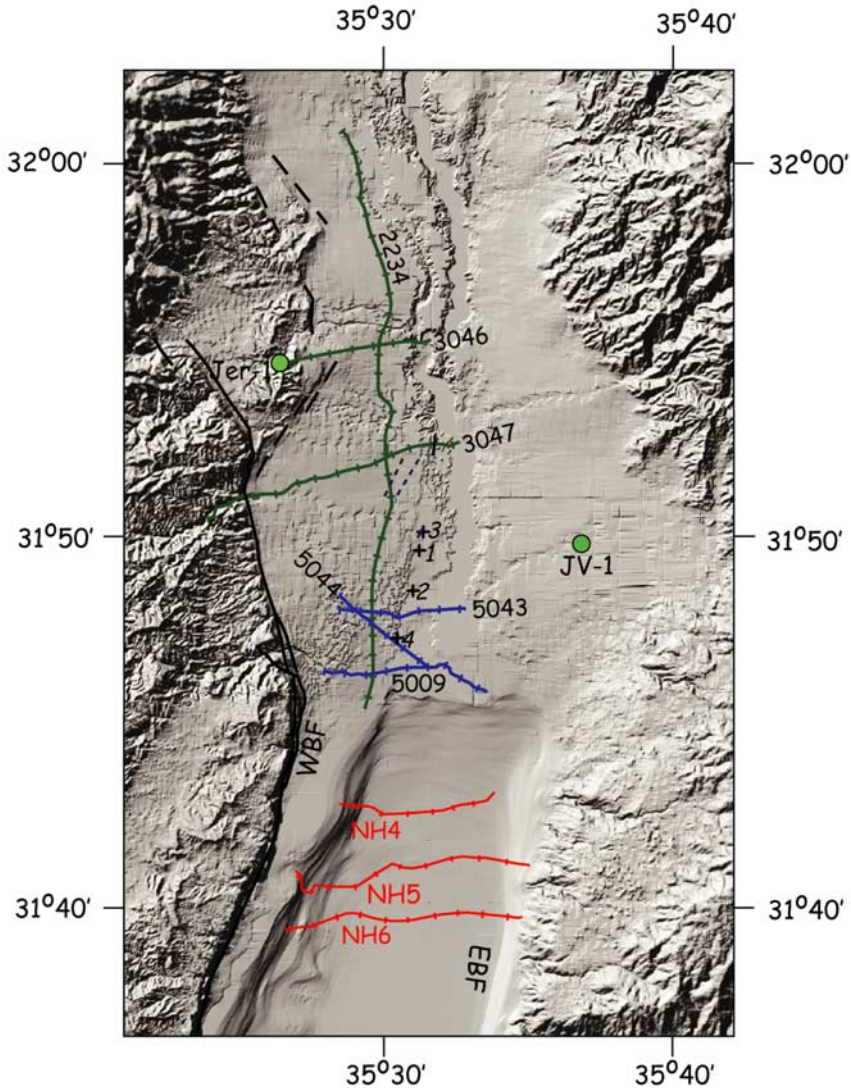

Figure 2. Data location. Black lines, onshore mapped faults; blue lines, high-resolution reflection lines; green lines, reprocessed exploration reflection lines; red lines, single-channel reflection lines [*Neev and Hall*, 1979]; black crosses, trench sites (1 and 2, *Reches and Hoexter* [1981]; 3, *Gardosh* [1987]; 4, *Shamir et al.* [2002] and S. Marco (personal communication, 2003)); green circles, boreholes with >1 km TD depth (JV-1, Jordan Valley-1; Jer-1, Jericho-1); WBF (EBF), western (eastern) boundary fault systems; DTM after *Hall* [1993].

with the initiation of transtensional motion in the Pliocene.

2. Data Acquisition and Processing

2.1. Seismic Reflection

[7] Two sets of seismic reflection data are used in this study (Figure 2):

[8] 1. Four high-resolution (HR) lines (5009, Figure 3; 5044, Figure 4; 5043, Figure 5; and 5035, not shown) are focused to a depth of 2.5–3.0 s TWTT (two-way travel time) (2.5–3.5 km). Field parameters are detailed in Table 1. Processing was based on the Focus software (Paradigm Geophysics). Prestack testing concentrated on attenuating shot-generated noise, improving the coherency of the data and the event character (broader bandwidth). The processing sequence and parameter tests included pre-decon testing, noise attenuation, deconvolution, elevation statics, velocity analysis, mutes and post stack coherence enhancement. The quality of the seismic signal was monitored at every stage of the processing.

[9] 2. Seven oil-exploration reflection lines which were reprocessed using the processing system

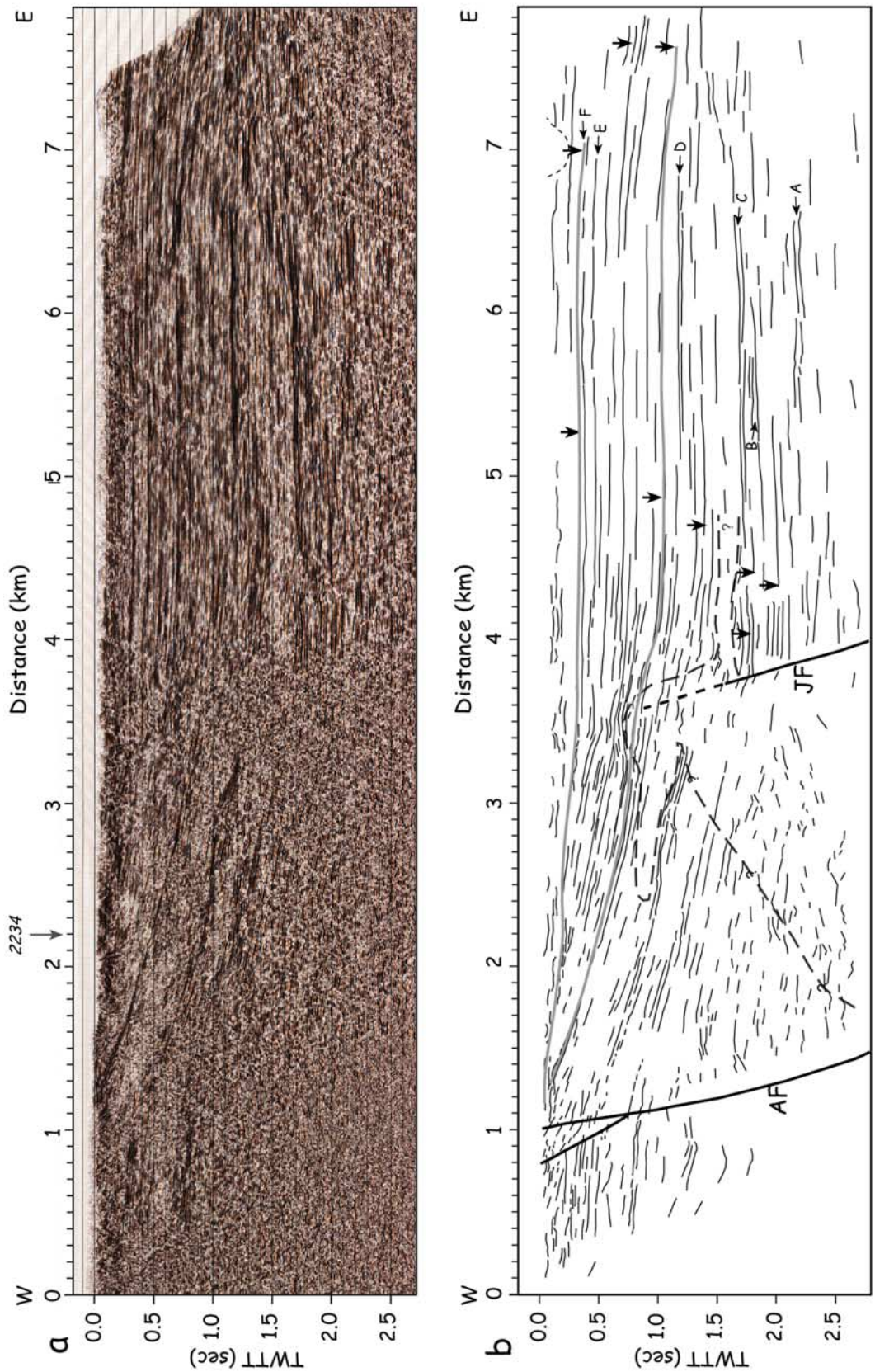

Figure 3. (a) Unmigrated time section and (b) interpreted section of high-resolution seismic reflection line 5009. JF, Jericho Fault Zone; AF, Almog fault. Specific reflector traces are shown in black, and interpreted chronostratigraphic horizons are shown in gray. The broken line marks the assumed extent of salt penetration. Horizons A through F are identified also in lines 5044 and 5043. Vertical arrows mark depocenters at specific horizons.

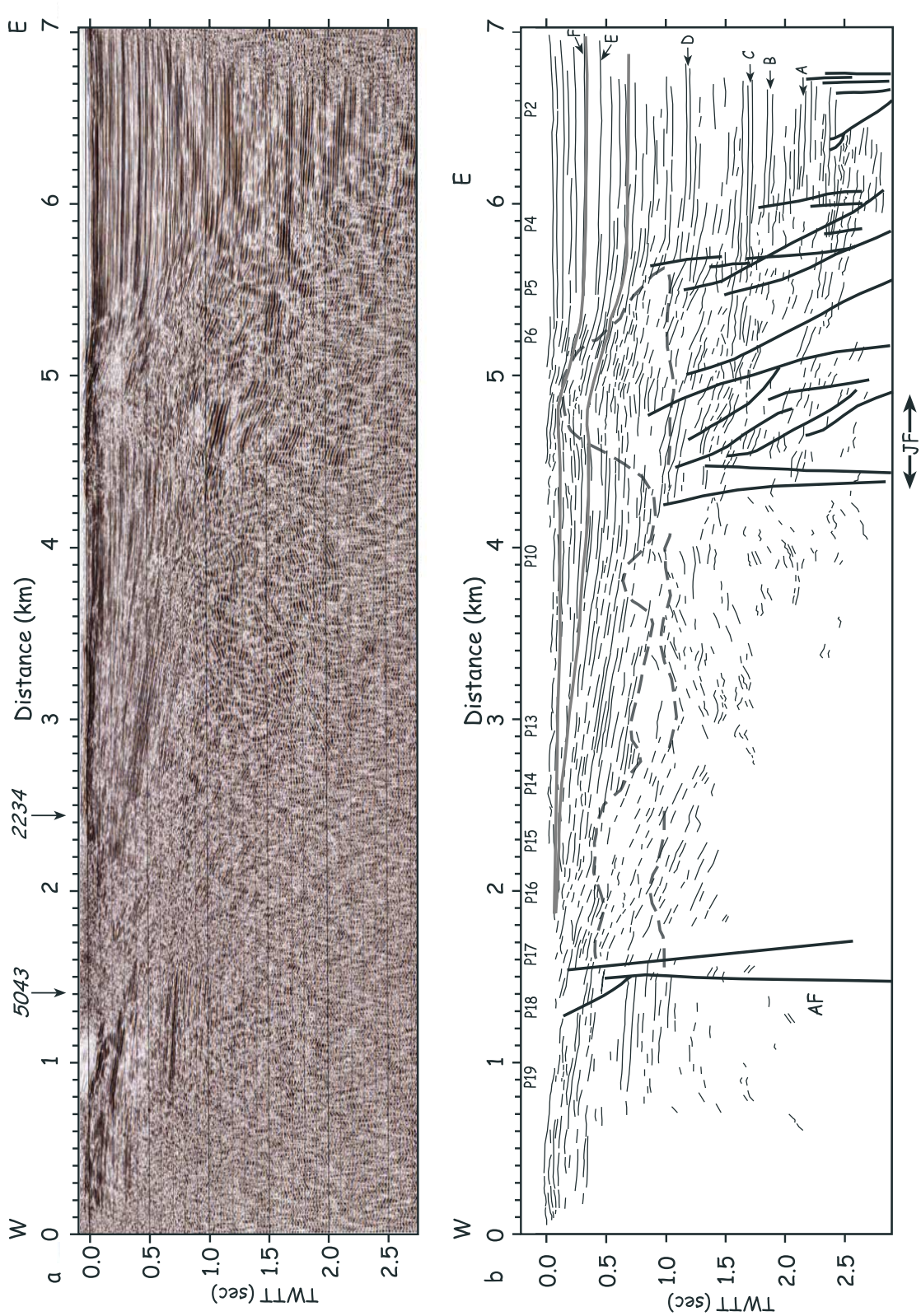

Figure 4. (a) Unmigrated time section and (b) interpreted section of high-resolution seismic reflection line 5044. JF, Jericho Fault Zone. Specific reflector traces are shown in black, and interpreted chronostratigraphic horizons are shown in gray. The broken line marks the assumed extent of salt penetration. Horizons A through F are identified also in lines 5009 and 5043.

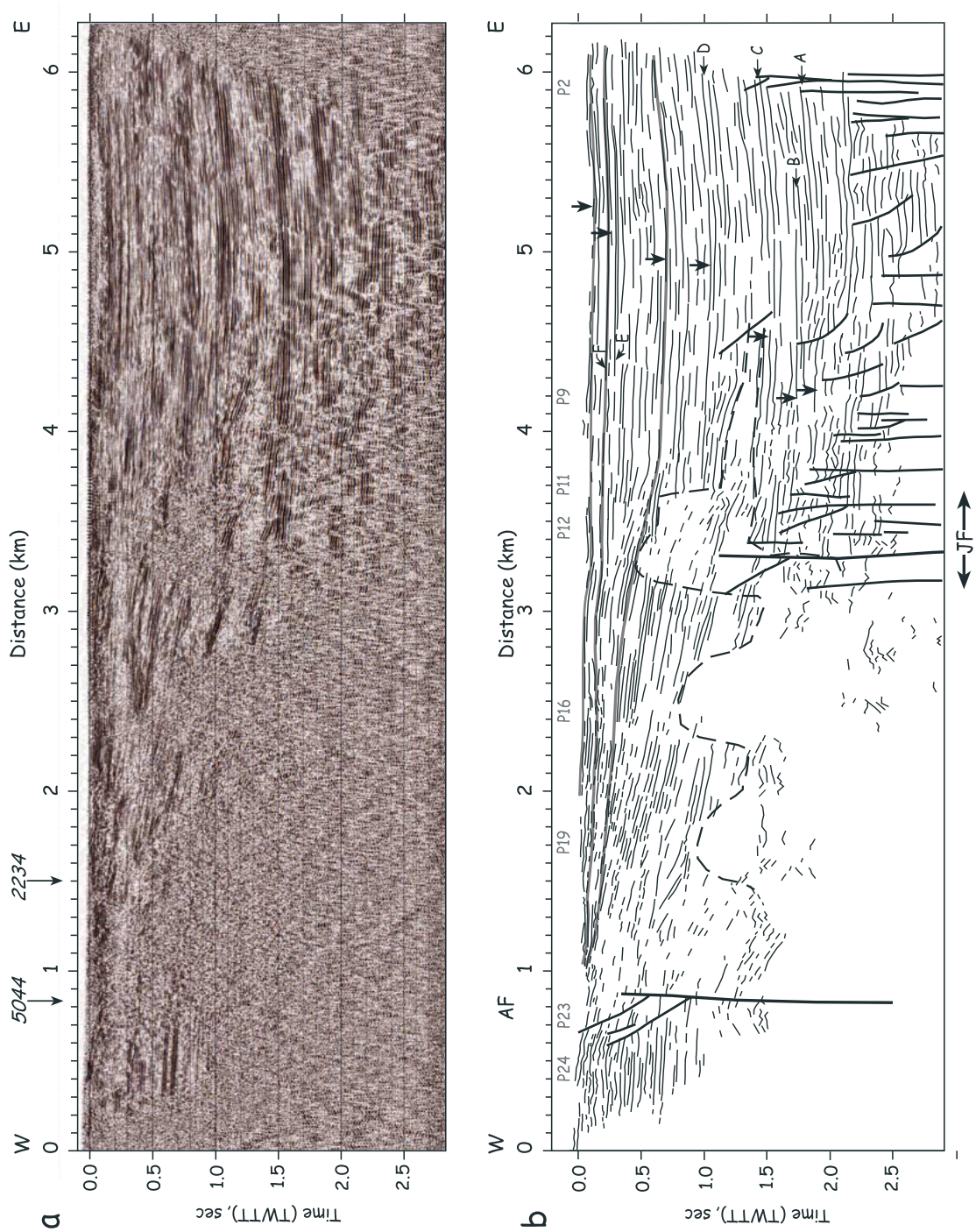

Figure 5. (a) Unmigrated time section and (b) interpreted section of high-resolution seismic reflection line 5043. JF, Jericho Fault Zone. Specific reflector traces are shown in black, and interpreted chronostratigraphic horizons are shown in gray. The broken line marks the assumed extent of salt penetration. Horizons A through F are identified also in lines 5009 and 5044. Vertical arrows mark depocenters at specific horizons.

Table 1. Acquisition Parameters of the Jericho Valley High-Resolution Reflection Lines

	Value/Description
Length, km	
5009 (Figure 3)	7.8
5044 (Figure 4)	7.0
5043 (Figure 5)	6.2
5035 (not shown)	1.63
Focus depth	2.5–3.0 s TWTT, 2.5–3.5 km
Energy source	1 vibroseis truck, 62,000 lb. pick-force
Cable	240 channels
Source interval	10 m
Geophone interval	10 m
Geophone frequency	10 Hz

ProMAX 7.2. The data comprised 93.2 km of seismic lines acquired in several periods (Table 2). The seismic source for all lines was vibroseis but field parameters varied. The main problems identified during the processing sequence were low signal-to-noise ratio, shot generated noise and static problems. Reprocessing procedures included elevation statics, deconvolution, velocity analysis, residual statics, migration, and post stack coherence enhancement. In this paper we present lines 3047 (Figure 6), 3046 (Figure 7) and 2234 (Figure 8).

[10] Following *Yilmaz* [2001], the vertical resolution of the seismic data is estimated as one quarter of the dominant wavelength λ, where $\lambda = \nu/f$, ν is the seismic velocity and f is frequency. Given the depth dependency of the seismic velocities in the study area (~1500 to ~5000 m/s) and of the dominant frequency (~60 to ~30 Hz) in the sampled rocks, and the group (geophone) intervals in the different lines, the estimated effective vertical resolutions range from 5–20 m for HR lines to 10–40 m for exploration lines (Table 3).

2.2. Seismicity

[11] The earthquake catalog used for the Dead Sea area is based on the Israeli (ISN) and the Jordanian (JSN) Seismic Networks [*Geophysical Institute of Israel*, 2004; *Natural Resources Authority*, 2004], both operating since the early 1980s. The two networks have been partly integrated as part of the peace treaty between Jordan and Israel in 1996, thus improving significantly the data resolution along the Dead Sea plate boundary.

[12] Over the last 20 years, 51 earthquakes with magnitudes $M_L \geq 2.5$ were recorded in the Dead Sea rift between latitudes 31°40′ and 32°13′. Catalog data were first augmented with additional P and S picks from both ISN and JSN and relocated by standard methods. Next, relative relocation was applied to the modified catalog, using the hypoDD algorithm [*Waldhauser and Ellsworth*, 2000] based on the double difference method. A 4-layer velocity model for this region [*Feigin and Shapira*, 1994] was used for epicenter determination and estimation of local magnitude based on coda duration [*Shapira*, 1988]. Results are shown in Figure 9 and listed in Table 4.

[13] Finally, single and composite fault plane solutions were calculated on the basis of P wave first arrivals, using the FPFIT program [*Reasenberg and Oppenheimer*, 1985] (Figure 9). Solutions were accepted or rejected on the basis of the number of polarity readings (minimum of 20), reasonable station azimuthal coverage and consistency in composite solutions (erroneously reversed station polarities). Station coverage, in particular, is a major limit in this region for low- to moderate-magnitude events.

3. Interpretation

3.1. Fault Structure and Seismicity

[14] Two major fault zones are observed in lines 5009, 5044, and 5043 (Figures 3, 4, and 5, respectively): The Jericho fault is the western boundary of the deep, eastern part of the basin separating a reflective eastern sequence from a nonreflective western sequence. It can be traced upsection only to horizon D. The basin as a whole is limited in the west by the Almog fault (Line 5009, Figure 3, x = 1 km; Line 5044, Figure 4, x = 1.5 km; Line 5034, Figure 5, x = 0.8 km). This fault strikes ~025°, merges with the western boundary fault system of the DSB further to the SSW (Figure 9) and is characterized by eastward subsidence and syntectonic deposition. The Almog fault is one of a series of faults trending 025°–030° (Figure 9) as follows: (1) The Nuweime fault (Figures 7 and 8), previously partly mapped by *Begin* [1973], merges with

Table 2. Reprocessed Seismic Reflection Lines

Line Number	Date Shot	Length, km
DS-3046 (Figure 6)	1982	7.03
DS-3047 (Figure 7)	1982	13.46
DS-3048 (not shown)	1982	13.46
SI-7101 (not shown)	1985	9.70
SI-7102 (not shown)	1985	9.75
SI-7103 (not shown)	1985	10.45
MI-2234 (Figure 8)	1994	29.40

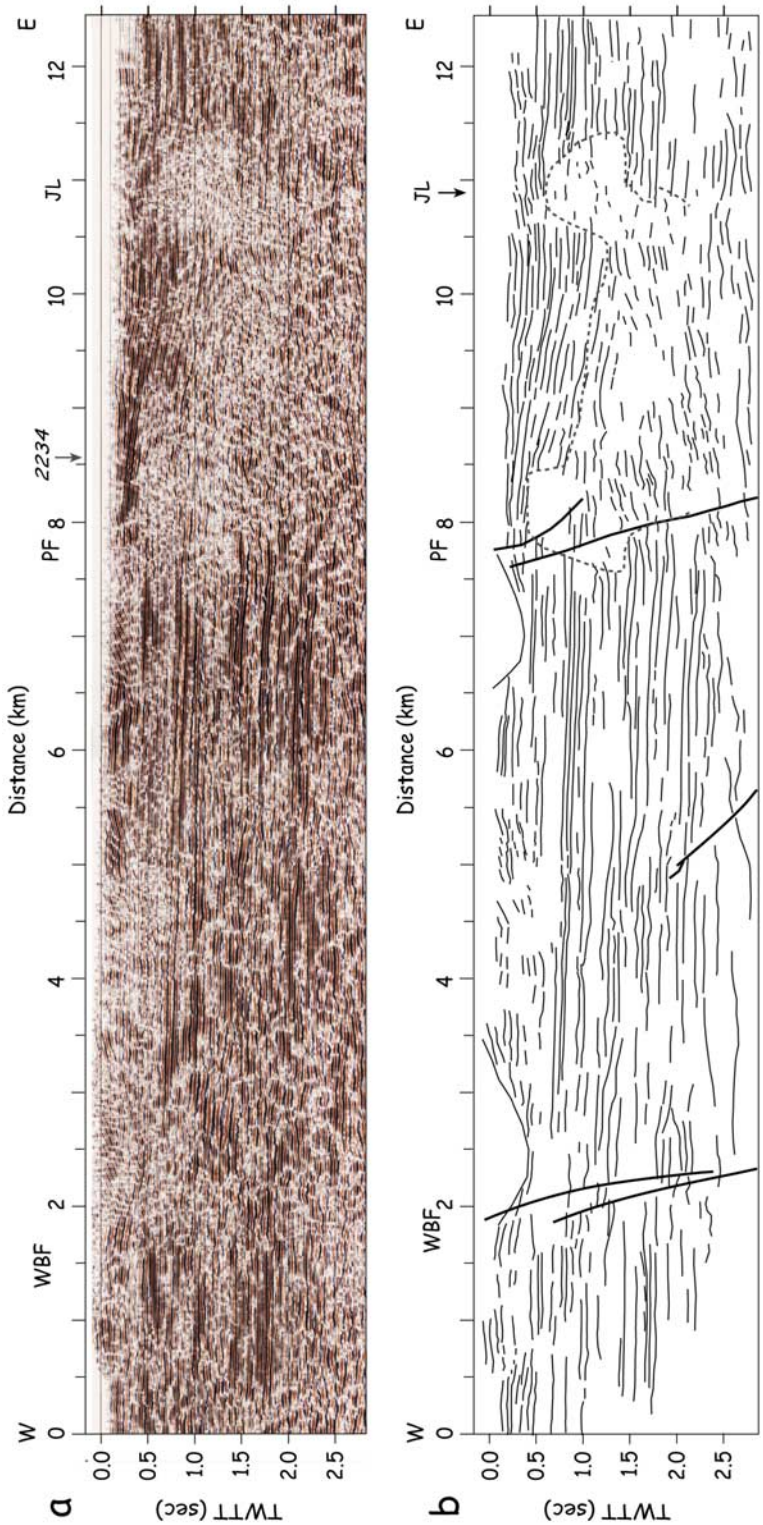

Figure 6. (a) Unmigrated time section and (b) interpreted section of reprocessed seismic reflection line 3047. WBF, Western Boundary Fault; PF, Perat fault; JL, Jericho lineament. Broken line indicates the assumed extent of the salt penetration.

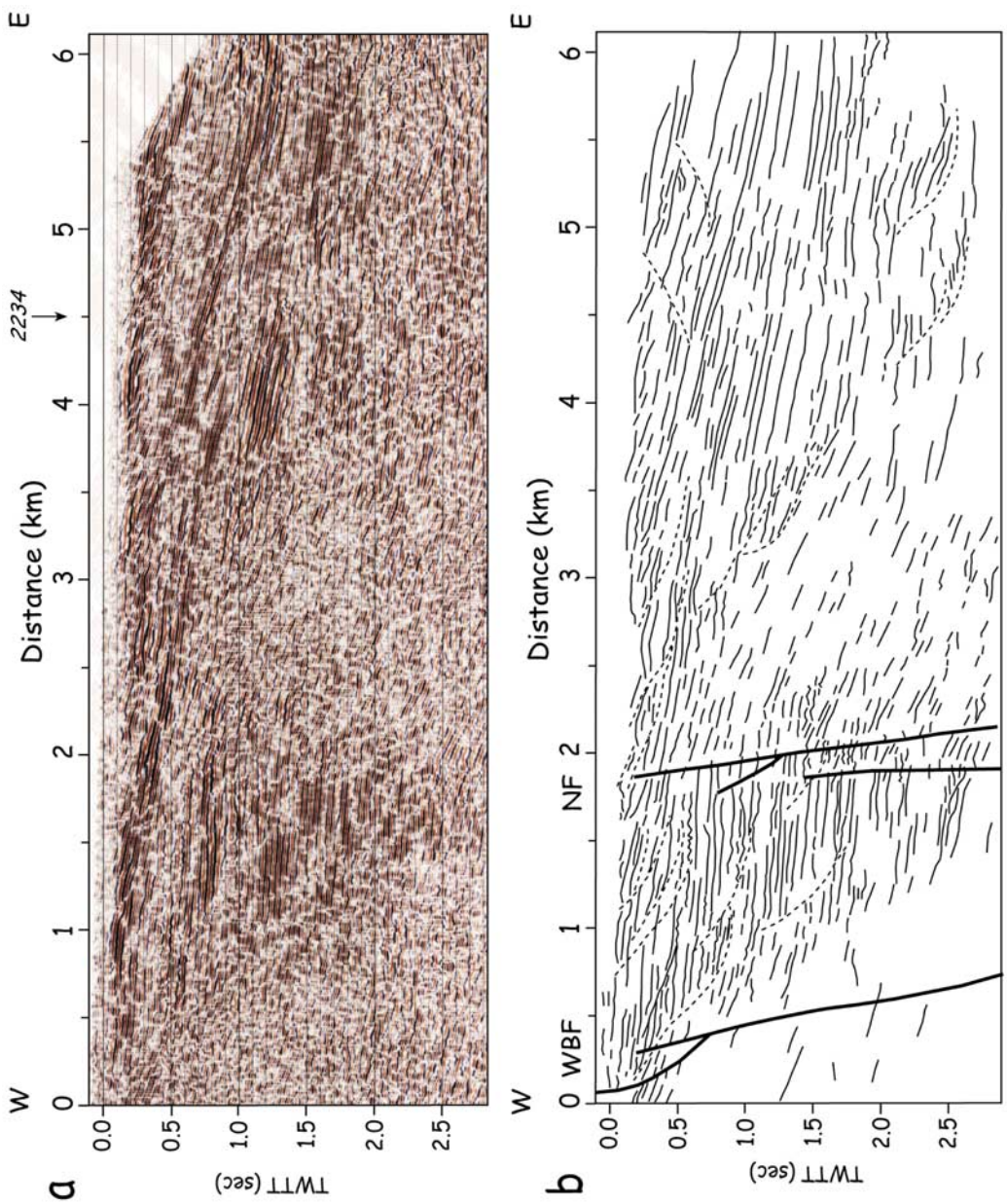

Figure 7. (a) Unmigrated time section and (b) interpreted section of reprocessed seismic reflection line 3046. NF, Nuweime fault; WBF, Western Boundary Fault. Stratigraphic identifications in the Jericho-1 borehole (located at the western end of the line; see Figure 2) are not shown as they cannot be correlated eastward.

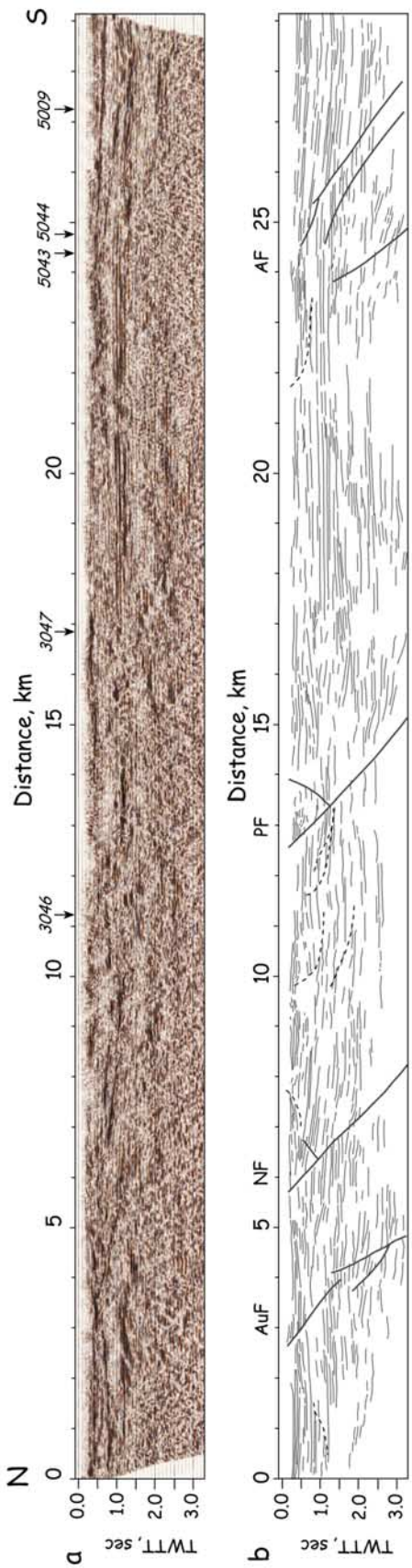

Figure 8. (a) Unmigrated time section and (b) interpreted section of reprocessed seismic reflection line 2234. AuF, Auja fault; NF, Nuweime fault; PF, Perat fault; AF, Almog fault.

the western boundary fault system. Seismicity shows that it is an active dextral-normal fault across the western-central Jericho Valley; (2) The Perat fault (Figures 6 and 8). The Nuweime-Perat fault system has a gravimetric signature (Figure 9), and apparently forms the northern boundary of the Dead Sea-Jericho basin. It is possible that events 40–43 are associated with this fault zone; (3) The Auja fault (Figure 8), observed also at the surface; (4) The Kalia fault trending 027° along the prominent scarp of the northwestern boundary of the Dead Sea basin [*Neev and Hall*, 1979] (Figure 9). This fault zone apparently extends southwestward and terminates onshore in the Darga Delta area [*Enzel et al.*, 2000]. Some of the February 2004 earthquakes in the northern Dead Sea basin occurred adjacent to the Kalia fault, some with dextral-normal mechanisms along its strike (Figure 9). The estimated location of the destructive 1927 $M_L \sim 6.2$ earthquake near the southern end of this scarp (Figure 1) [*Shapira et al.*, 1992] makes the Kalia fault the prime candidate for this event. More work is needed to elucidate the geometrical relations between the Jericho fault and the NNE-trending fault system. Geomorphic features near the intersection between the Jericho and Almog faults are ambiguous, but the strike of the Almog fault is apparently more consistent with the gravity field gradient. It is possible that the distributed fracturing observed east of the Jericho fault in lines 5044 and 5043 (Figures 4 and 5) is related to the NNE extension of the Kalia fault.

[15] The relocated epicenter distribution shows no distinct clustering, neither along a major DST segment nor along the Jericho Lineament. Most current earthquake mechanisms in this part of the DST zone show a bimodal orientation distribution, with NNE-NE dextral-normal and NW-NNW sinistral-normal nodal planes, and only minor occurrence of NE or NW oriented normal faults and

Table 3. Effective Vertical Resolution of Seismic Data in This Study

TWTT, s	High-Resolution Lines (gr. int. = 10 m)	Petroleum Lines (gr. int. = 35–45 m)
	Shallow-Medium	
0 to 1.5–2.0	~5 m	10–20 m
	Deep	
1.5–2.0 to 2.5–3.0	8–10 m	35–40 m

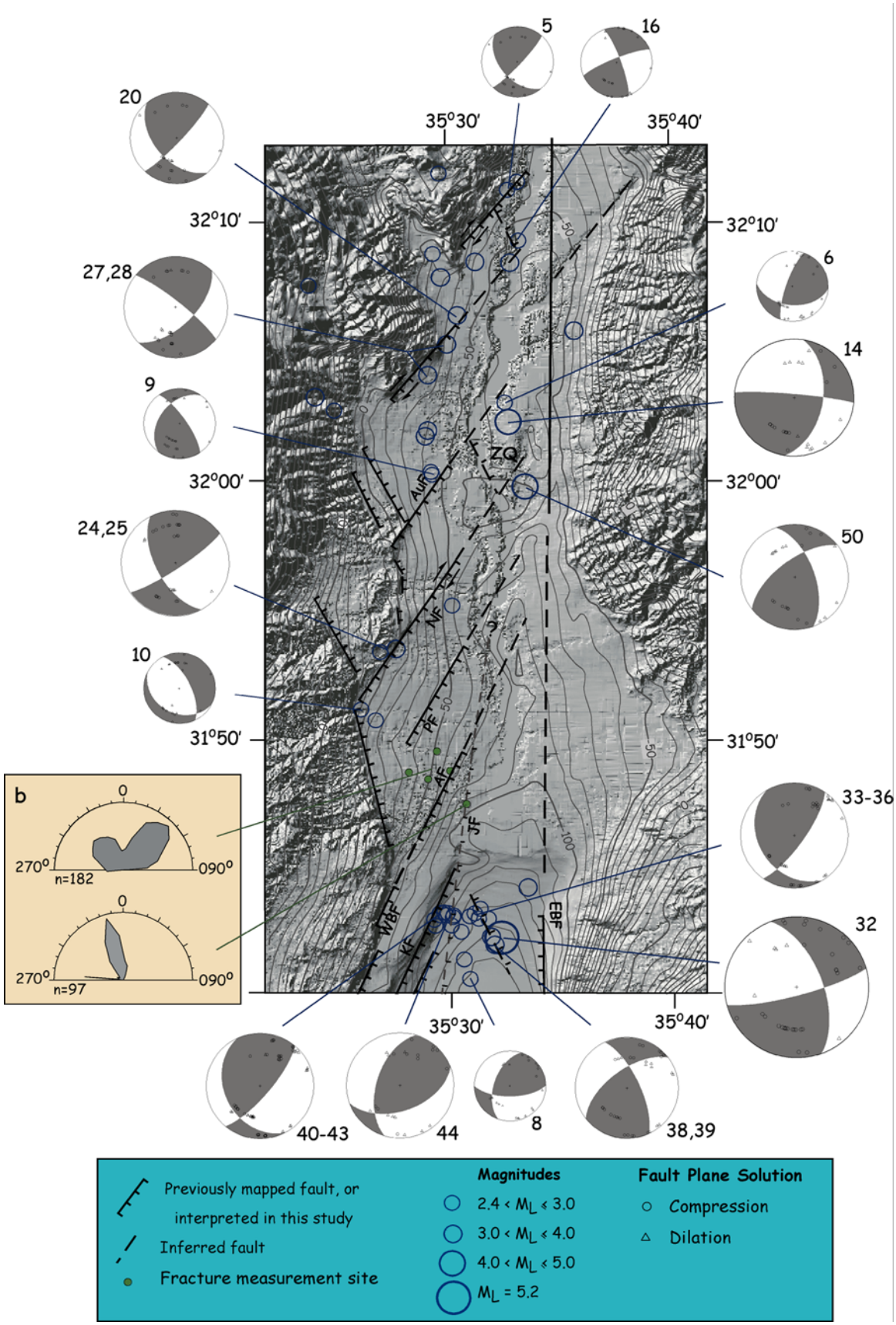
5
16
20
35°30′
35°40′
32°10′
32°10′
6
27,28
14
9
32°00′
32°00′
24,25
50
10
31°50′
31°50′
33-36
32
35°30′
35°40′
40-43
44
8
38,39
b
0
270°
090°
n=182
0
270°
090°
n=97
AuF
ZQ
NF
PF
AF
JF
WBF
KF
EBF
Previously mapped fault, or interpreted in this study
Inferred fault
Fracture measurement site
Magnitudes
2.4 < ML < 3.0
3.0 < ML < 4.0
4.0 < ML < 5.0
ML = 5.2
Fault Plane Solution
Compression
Dilation

Figure 9

Table 4. Relocated Earthquakes in the Jericho Valley

	Origin Time							
	Year	Month	Day	hr:min:sec	M_L	Latitude, °N	Longitude, °E	Depth, km
1	1984	11	5	51:01.2	3.6	32.141	35.380	10.00
2	1985	8	17	05:12.3	2.9	32.057	35.409	12.00
3	1986	2	4	19:57.6	2.8	32.193	35.549	2.27
4	1986	11	24	51:06.9	2.5	32.080	35.587	6.00
5	1988	1	30	00:00.7	2.3	32.188	35.542	15.33
6	1990	11	16	56:04.2	2.6	32.050	35.530	17.92
7	1991	12	29	38:23.2	3.3	32.088	35.497	3.57
8	1992	4	23	59:44.3	2.8	31.678	35.513	16.21
9	1993	1	1	47:00.3	2.8	32.005	35.485	1.00
10	1993	7	4	05:52.4	2.7	31.852	35.433	1.36
11	1994	2	12	28:04.5	2.7	32.004	35.486	0.56
12	1994	5	7	11:50.4	2.7	31.845	35.444	1.11
13	1994	5	30	48:09.3	2.7	32.198	35.491	12.56
14	1994	9	16	18:56.2	4.1	32.038	35.533	21.48
15	1995	1	22	06:21.8	2.5	32.146	35.487	4.76
16	1996	5	22	08:40.4	2.8	32.150	35.560	12.29
17	1997	11	17	29:54.2	3.2	32.054	35.400	3.43
18	1998	1	19	04:26.1	2.3	32.045	35.414	3.42
19	1998	8	17	43:15.6	2.6	31.919	35.500	18.76
20	2000	3	11	52:31.1	3.1	32.107	35.505	2.98
21	2000	3	27	05:47.9	2.6	31.723	35.521	17.53
22	2000	3	28	03:18.2	2.9	31.717	35.527	16.80
23	2000	5	11	35:16.2	3.0	32.096	35.591	14.21
24	2001	9	22	13:29.6	2.4	31.890	35.443	7.68
25	2001	9	22	34:48.2	3.1	31.891	35.459	7.35
26	2001	12	20	05:56.9	3.1	31.737	35.556	13.08
27	2002	2	24	56:01.2	3.6	32.068	35.483	3.41
28	2002	6	17	19:06.2	3.3	32.107	35.463	10.90
29	2002	7	5	46:22.4	3.0	32.141	35.518	1.98
30	2002	8	13	28:25.6	2.8	32.126	35.395	6.76
31	2002	10	14	51:54.3	3.3	32.141	35.544	18.95
32	2004	2	11	15:03.2	5.2	31.705	35.536	17.07
33	2004	2	11	09:15.0	2.7	31.720	35.516	14.75
34	2004	2	11	33:51.1	2.7	31.712	35.488	14.65
35	2004	2	11	31:17.1	2.8	31.721	35.497	16.15
36	2004	2	11	36:13.9	2.7	31.717	35.519	16.48
37	2004	2	12	09:41.3	2.7	31.718	35.501	15.89
38	2004	2	13	23:21.9	2.8	31.708	35.507	15.96
39	2004	2	13	02:36.5	3.6	31.705	35.529	16.81
40	2004	2	19	18:01.4	2.7	31.713	35.499	16.63
41	2004	2	19	47:35.5	2.8	31.718	35.513	15.45
42	2004	2	20	46:41.7	2.8	31.719	35.501	16.21
43	2004	2	20	04:04.3	2.5	31.721	35.494	16.57
44	2004	2	24	11:32.5	3.1	31.720	35.492	16.64
45	2004	5	13	56:29.3	2.8	31.719	35.496	14.91
46	2004	5	25	17:52.9	2.6	31.691	35.509	15.38
47	2004	5	31	35:46.0	2.9	31.716	35.487	15.19
48	2004	5	31	52:38.3	3.2	32.032	35.483	4.02
49	2004	6	3	18:52.1	3.2	32.028	35.481	3.05
50	2004	7	7	35:08.0	4.6	31.974	35.574	16.90
51	2004	7	9	16:28.4	3.6	31.700	35.531	16.98

Figure 9. (a) Relocated epicenters, focal mechanisms (see Table 4), and interpreted fault structure (schematic) in the Jericho Valley section of the DST, superimposed on the gravity (Bouguer) anomaly map [*ten Brink et al.*, 1993]. EBF and WBF, eastern and western boundary fault systems, respectively; ZQ, Zahrat el-Qurein; JF, Jericho Fault; AF, Almog Fault; PF, Perat Fault; NF, Nuweime Fault; AuF, Auja Fault. (b) Fracture orientation distribution in the Jericho Valley (top, *Gardosh* [1987]; bottom, *Shamir et al.* [2002]). DTM after *Hall* [1993].

N-S sinistral-normal mechanisms. This is consistent with the orientation distributions of fractures, joints and veins in Pleistocene beds recorded in the southern Jericho valley [*Gardosh*, 1987] and in sites along the Jericho Lineament [*Shamir et al.*, 2002], where subvertical fractures, occasionally striated and filled with crystalline gypsum and breccia, were found in silty clay layers of the Pleistocene Amora formation.

[16] The M_L5.2 earthquake of 11 February 2004 in the northern DSB (event 32, Table 4 and Figure 9) was the largest to occur in the northern Dead Sea basin since the destructive 1927 $M_L \sim 6.2$ earthquake. It was followed by a cluster of 27 nearby events of $M_L = 2.0–3.7$ in the following 5 months. Our preliminary analysis does not reveal a clear epicenter lineation of this cluster, specifically not along one of the boundary fault systems. Furthermore, the calculated fault plane solutions show that this cluster is consistent with the general dominance of the bimodal NE-NW nodal plane pattern. The NNW-oriented, sinistral-normal nodal plane of the M_L5.2 event therefore seems preferable.

3.2. Sedimentary Basin

[17] The high-resolution lines (5009, 5044 and 5043; Figures 3–5) provide cross sectional images of the south-central Jericho valley. The valley is occupied by the eastward deepening Jericho Basin, filled with a sedimentary sequence cut by unconformities of various scales. The lack of sufficiently deep nearby borehole data prevents absolute stratigraphic identification of the observed reflectors and, specifically, identification of the top of the prerift (i.e., pre-Neogene) ''basement''. *Rotstein et al.* [1991] suggested that this basement lies at a depth of ~125 m in the central Jericho Valley, based on a single, well-preserved Eocene fragment from a water drillhole. Reexamination of the same cutting assemblage (A. Almogi-Lavin, personal communication, 2000) revealed a mixture of poorly preserved Eocene and upper Cretaceous fragments, representing the clastic basin fill.

[18] Six interpreted chronostratigraphic horizons (A–F) are identified and correlated between the HR lines and several horizons (gray lines) are traced across the basin (Figures 3–5). Horizon D, at a depth of ~1–1.2 s TWTT, marks a transition from a deep sequence of low-frequency, faulted and disrupted reflectors to a shallow sequence of more finely layered, generally un-faulted, high-frequency reflectors. In the deeper, pre-D sequence, massive eastward prograding sedimentary prisms are seen, e.g., in line 5009 (Figure 3), (x, t) = (4.2, 1.3), line 5044 (Figure 4), (x, t) = (5.5, 1.1) and line 5043 (Figure 5), (x, t) = (3.8, 1.1). On the basis of seismic character only, we speculate that the D horizon marks the top of the fluvial-clastic, middle-late Miocene Hatzeva formation, or lies within the Plio-Pleistocene Amora Fm., possibly at the top of its lower, sandy member. This cannot be confirmed at this time due to the lack of borehole data. The Jericho fault limits the deep sequence to the eastern part of the basin while the shallow sequence extends westward, to the Almog fault. The basinal depocenter of the pre-D sequence is adjacent to the Jericho fault, indicating that this was the major active fault at that time.

[19] The post-D sequence consists of finely bedded, high-frequency reflectors that are interpreted as the Pliocene-Holocene sequence of lacustrine and evaporitic sediments. Thus the D unconformity apparently marks a major transition from terrestrial-fluvial to lacustrine depositional conditions. This was accompanied by an eastward shift of the basinal depocenter, expressed, for example, by eastward subsidence and thickening at the eastern end of line 5009 (Figure 3). Two distinct reflectors, E and F, are identified in the post-D sequence. Assuming an average P wave velocity of 1500–2500 m/s, the depth of reflector F is roughly 520–870 m below mean sea level, i.e., nearly the depth of the current Dead Sea bottom (−730 m below mean sea level [*Neev and Hall*, 1979]).

[20] The abundance and depth of unconformities and cut-and-fill structures in the inner basin suggests that its fill extends to a depth of at least ~2.5 s TWTT, i.e., ~2–3 km. Note in particular the prominent unconformity at (x, t) = (6, 2.5) in line 5044 (Figure 4).

[21] A systematic eastward decrease of depth-gradients of the mean stack velocity (MSV) in the HR lines (Figures 10a and 10c) is interpreted as reflecting a gradually increasing proportion of fine, most likely lacustrine, components toward the Jericho basin depocenter. North of the Almog fault, apparently continuous reflector packages (e.g., at (x, t) = (5–7, ~0.8) in line 3047, Figure 6, and (x, t) = (17–25, ~1) in line 2234, Figure 8) were previously interpreted as upper Cretaceous ''basement'' rocks (L. Fleischer, personal communication, 2001). However, sedimentary structures that underlie these reflectors (e.g., at (x, t) = (5–5.5, ~1.4) in line 3047 and (x, t) = (17–19, ~1.4) in line 2234), and the abundance and depth of unconformities (e.g., line 5044, Figure 4, (x, t) =

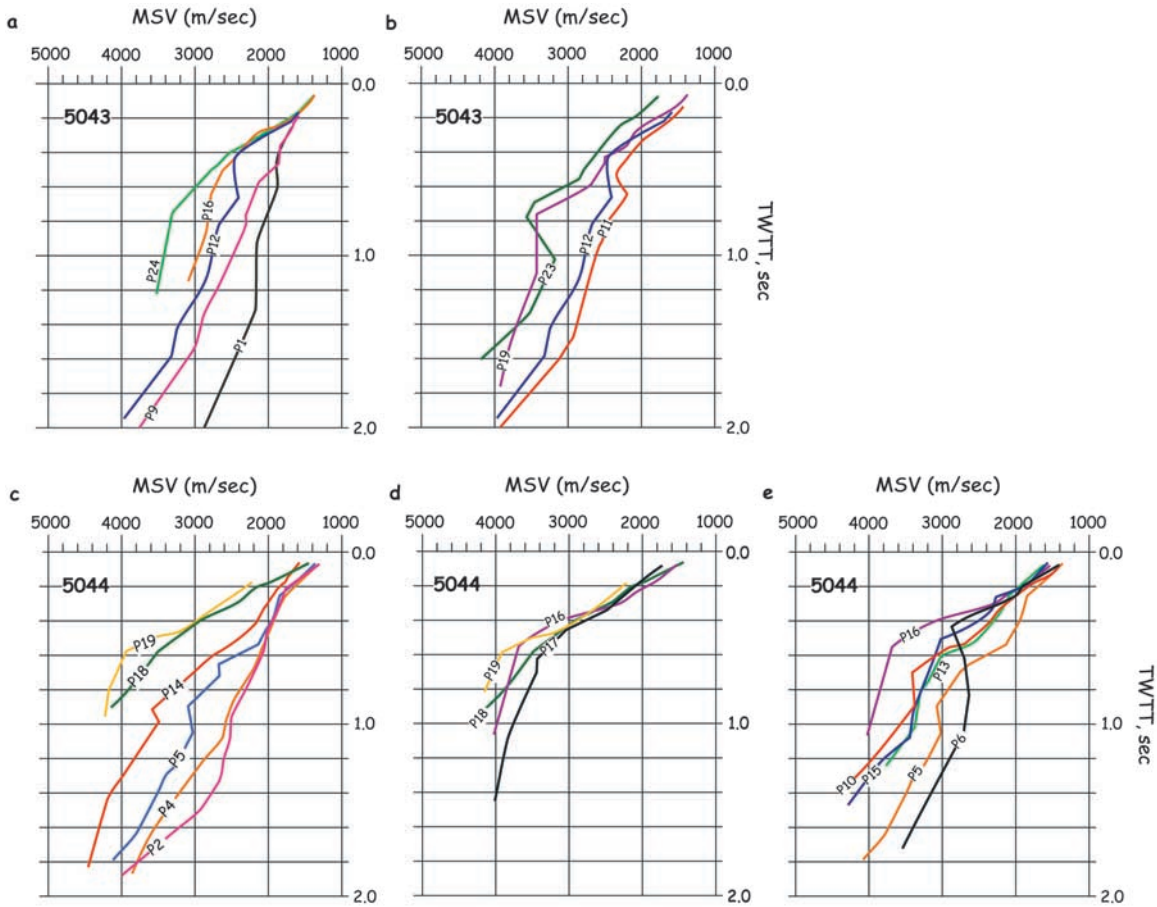

Figure 10. Profiles of the stack velocity along seismic reflection lines (a and b) 5044 and (c–e) 5043. Profile locations are shown in Figures 4 and 5.

(6, 2.5)), question this identification. The only nearby deep borehole is Jericho-1 (Figure 2) [*Shertok*, 1980], at the western end of line 3046 (Figure 7), where Mesozoic rocks (down to the mid-Jurassic Zohar formation at 1891 m) were previously identified. However, the location of the borehole west of the main rift boundary fault (Figure 2) prohibits correlation with the eastern side of the fault, where coherency is lost and discontinuous and unconformable reflectors dominate, with abundant upward concave, eastward facing channel cuts associated with contorted and fragmented reflectors. Eastward cyclic basin filling is observed, with syntectonic deposition east of the Nuweime fault (NF).

3.3. Salt Diapirism

[22] The Jericho basin is divided into two subbasins along the trace of the Jericho fault (Figures 3–5). The boundary zone (Line 5009, Figure 3, x = 3.2–3.9 km; line 5044, Figure 4, x = 4.6–5.2; line 5043, Figure 5, x = 3.1–3.8 km; line 3047, Figure 6, x = 7.5–11.5 km) is marked by higher acoustic transparency and by several characteristic features that are interpreted as salt-related structures [*Trusheim*, 1960]:

[23] 1. Upward deflected reflectors at the zone margins, forming local synformal structures (Line 5044, Figure 4, (x, t) = (4.3, ~0.5) and (5.5, ~0.6); Line 5043, Figure 5, (x, t) = (3.8, ~0.6); Line 3047, Figure 6, (x, t) = (10.4, ~0.7) and (11.5, ~0.7)). These are interpreted as rim synclines off the salt swell that typically develop prior to and at the initiation of the diapiric stage, due to salt withdrawal or upward drag.

[24] 2. Antiformal structures (Line 5009, Figure 3, (x, t) = (~3.5, ~0.7); Line 5044, Figure 4, (x, t) = (4.5–5, 0–1.0)) formed by uplift of overlying layers, where passive extensional collapse is typically observed.

[25] 3. A pseudo-anticline (Line 5043, Figure 5, (x, t) = (3, ~0.5)), lying on a flat horizon with downward decaying amplitude and maximum

thickness under its crest. Such structures form due to sinking of the horizons adjacent to the salt body as withdrawal proceeds [*Vendeville and Jackson*, 1992].

[26] 4. Occasional anomalously high values of the mean stack velocity (MSV) (e.g., profiles 11 and 12 in Figure 10b; profiles 5 and 6 in Figure 10e), which are interpreted to reflect anomalously high physical velocities. In the Dead Sea basin, average P wave velocities of salt are ~3500 m/s compared with 1500–2500 m/s for the Pliocene-Holocene basinal sediments in which the salt layers are embedded [*Ezersky*, 2003].

[27] Salt bodies in the DSB are layered and interbedded with carbonate, shale and gypsum layers. As observed at the surface in the large Mt Sedom diapir, these sequences are distorted, tilted and fractured due to diapiric motion, resulting in short wavelength features that are observed in the high-resolution data presented here. This explains why previously documented salt bodies in the DSB, identified on the basis of low-resolution exploration or single-channel lines, seemed less reflective. In addition, 3-dimensional wave propagation often causes apparent reflections which may be particularly pronounced when the velocity contrast with the actual country rock (salt, in this case) is higher.

[28] Notably, these features are observed also in the northern Jericho basin, in line 3047 (Figure 6, x = 11 km), where the Jericho fault itself cannot be clearly identified. Thus these observations are interpreted to reflect an elongated salt diapir that rises along the Jericho fault. As shown in Figures 3–6, the salt apparently extends westward, possibly as far as the Almog (Figures 3–5) and Perat (Figure 6) faults. The more pronounced onlap relations and reflector deflection on the eastern side of the salt body are attributed to the asymmetric subsidence across the salt diapir. Finally, the described salt-related observations are qualitatively similar to observations made around the Sedom diapir in the southern Dead Sea basin [*Al-Zoubi and ten Brink*, 2001; *Gardosh et al.*, 1997].

4. Discussion

[29] Integration of the data presented above suggests that the Jericho Valley section of the Dead Sea Transform evolved from a localized to a distributed fault structure, the change presumably taking place in the Pliocene. Prior to this change, the central-eastern part of the Jericho Valley was occupied by a narrow, fault-bounded inner basin, bordered on the west by the Jericho fault (Figures 3–5). Within this basin, low-frequency, high-amplitude reflector packages, interpreted as mostly fluvial-clastic units, show eastward thickening, onlap and angular unconformities, indicating high-energy flow with a west-to-east component of motion. Several seismically transparent zones within this sequence presumably represent salt layers or other halokinetic disruptions of the reflector continuity. The depocenter during the period represented by this sequence was at the western side of the basin, adjacent to the Jericho fault, indicating that this was the major active fault in this section of the DST at the time. Furthermore, the single-channel reflection profiles collected by *Neev and Hall* [1979] suggest that the Jericho Valley inner basin extended southward, into the current northern Dead Sea basin. These profiles (Figure 11) show an inner buried basin bounded on the west by the Jericho fault that is covered by westward onlapping layers and associated with a local depocenter that shifted eastward after the cessation of activity. These observations strongly resemble those in Figures 3–5; nevertheless, an accurate depth correlation between the two data sets is not possible at this time because of the vast difference in resolution, the uncertainty in stratigraphy and seismic velocities and the unknown thickness of the Jordan River Delta. The thickness of the inner basin fill (presumably Neogene-Pliocene) cannot be determined directly, but abundant sedimentary structures, including a prominent, eastward inclined unconformity near the bottom of the imaged section in line 5044 (Figure 4, (x, t) = (6.2, 2.5)), suggest that it is at least 2.5–3 km deep.

[30] The high-resolution reflection data from the southern Jericho Valley show that the inner basin, as well as the Jericho fault, is topped by a distinct reflector package, horizon D, which marks a major sedimentary and tectonic change. The age of this horizon is not clearly constrained due to the lack of sufficiently deep borehole data and the uncertainty in seismic velocities. For average P wave velocities of 1500–2500 m/s, its depth can be in the range 900–1500 m below mean sea level, respectively (base datum for all HR lines is −400 m msl). On the basis of seismic character, including the interpretation of low-reflection areas as representing salt, we hypothesize that horizon D lies near the top of the Pliocene Sedom formation or within the Plio-Pleistocene Amora formation.

[31] Horizon D is unconformably overlain by a thick sequence of high-frequency, finely layered

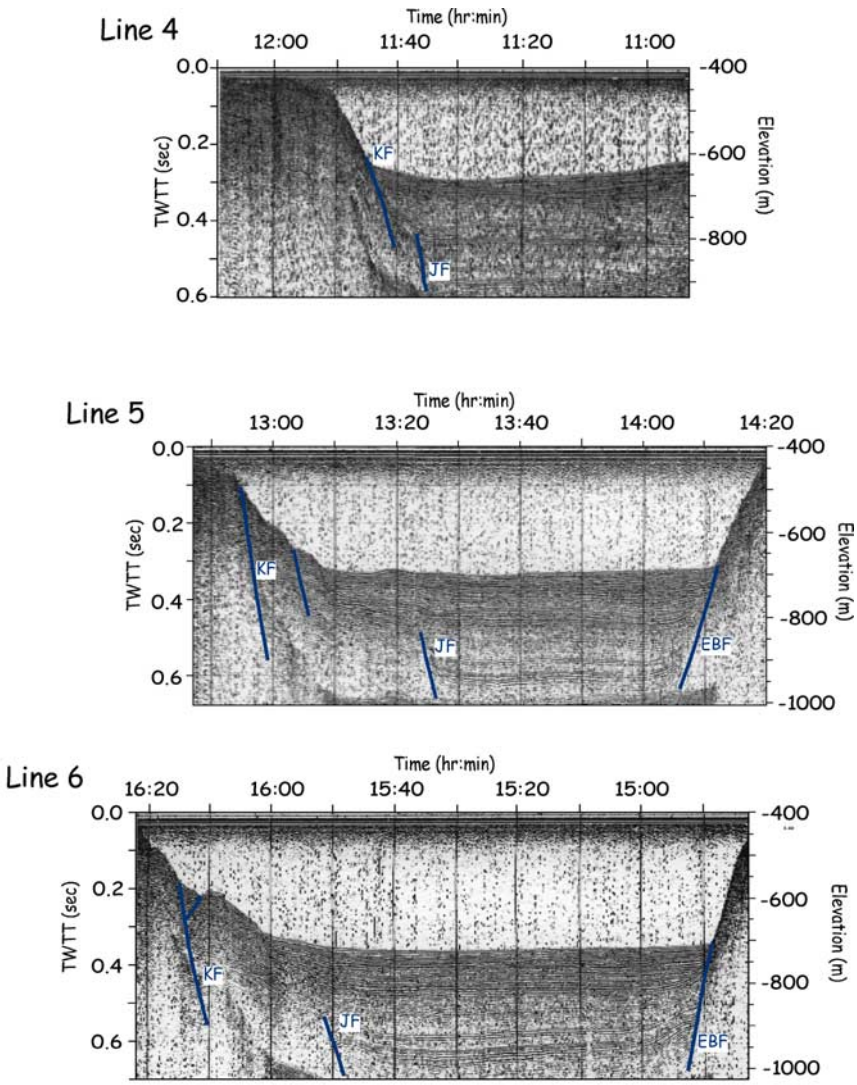

Figure 11. Single-channel reflection profiles 4–6 of *Neev and Hall* [1979] and suggested fault interpretations. JF, Jericho fault; KF, Kalia fault; EBF, Eastern Boundary Fault.

reflectors apparently deposited under low-energy conditions over the entire width of the Jericho basin, to the Almog (Figures 3–5 and 8), Perat (Figures 6 and 8) and Nuweime (Figures 7 and 8) faults in the west. The syntectonic nature of the deposition of this, apparently lacustrine-fluvial sequence, is expressed in sedimentary prisms formed over the downfaulted blocks to the east of these faults. The primary basin subsidence motion shifted eastward, as expressed by the general eastward migration of depocenters, indicating the increasing role of the eastern boundary fault. Note in particular the clear eastward thickening sequence unconformably overlying horizon D at the far eastern part of line 5009 (Figure 3). Normal offset across the major eastern fault may be responsible for the dramatic increase in basin-fill thickness, from 274 m in the Jordan Valley-1 borehole (Figure 2) [*Bender*, 1968] to several kilometers in the center of the basin (Figures 3–5). Further north, this fault is expressed in N-S fracturing and colinear solution holes east and north of Zahrat el-Qurein (Figure 1) [*Belitzky and Mimran*, 1996].

[32] The post-D sequence is disrupted by several low-reflection areas, interpreted as salt bodies that apparently utilized the Jericho fault zone as a conduit for diapiric motion and ascended above it. We suggest that this caused the uplift, passive collapse (normal faulting) and deformation of Late Pleistocene and Holocene sediments observed at the surface and in trenches along the Jericho Lineament [*Reches and Hoexter*, 1981; *Gardosh*,

1987; *Gardosh et al.*, 1990; Z. Garfunkel, personal communication, 2003]. Indeed, these observations are limited to a ~15 km long zone and disappear southward toward the Dead Sea basin (e.g., at trench site 4, Figure 2; S. Marco, personal communication, 2003). Thus the salt-induced surface features trace the deep-seated Jericho fault but do not express its current activity, certainly not as a major segment of the DST. Considering the abundance of salt diapirs in the DSB [*Zak*, 1967; *Neev and Emery*, 1967; *Neev and Hall*, 1979], the presence of salt bodies in the Jericho basin (suggested also by *Belitzky and Mimran* [1996]) expresses their tectonic and sedimentary continuity. If the Pliocene salt formation extends throughout the Jericho basin, it is possible that the deflection of the gravity field contours (around 31°50′N/35°32′E in Figure 9) and the upward concave form of the layers (e.g., line 5043, Figure 5) to the east of the Jericho lineament reflect salt withdrawal.

[33] In summary, the tectonic change associated with the post-D depositional change seems to have involved delocalization of the transform motion. Cessation of shear along the N-S striking Jericho fault was accompanied by appearance of a penetrative strain field expressed by a bimodal distribution (NW-NNW and NNE-NE) of fault systems, post-Pleistocene fracture sets and recent earthquake mechanisms. This strain field has prevailed across a broad zone, involved normal extension and resulted in the wide transform basin observed today. Its persistence to the present is expressed by current microseismicity. This tectonic evolution is consistent with the change from pure strike slip to transtensional motion across the DST in the Pliocene (~5 Ma), due to a 5° eastward shift of the Africa/Arabia Eulerian pole of rotation [*Quennell*, 1959; *Garfunkel*, 1981; *Joffe and Garfunkel*, 1987]. This involved increased divergence across this plate boundary and broadening of the DST in the Jericho Valley, and implies a post 5 Ma age for horizon D.

[34] Accepting that the NNE-trending faults are normal-dextral and leaning against a major eastern DST segment, the mechanics of the post-D fault system in the Jericho Valley can be described as a version of the "bookshelf" pure shear mechanism [*Mandl*, 1987] (Figure 12), with two major differences: (1) Only one major boundary fault, in the east, is observed, and the overall motion across the plate boundary is partitioned between left-lateral strike slip motion along this fault and distributed shear and counterclockwise rotation across a 10–20 km wide zone west of it. (2) In general, a bookshelf mechanism represents pure shear and should result in axial extension and transverse convergence. The Jericho Valley, however, is clearly tensile in both the axial direction (consistent with gravity modeling along the DST [*ten Brink et al.*, 1993] and the transverse direction.

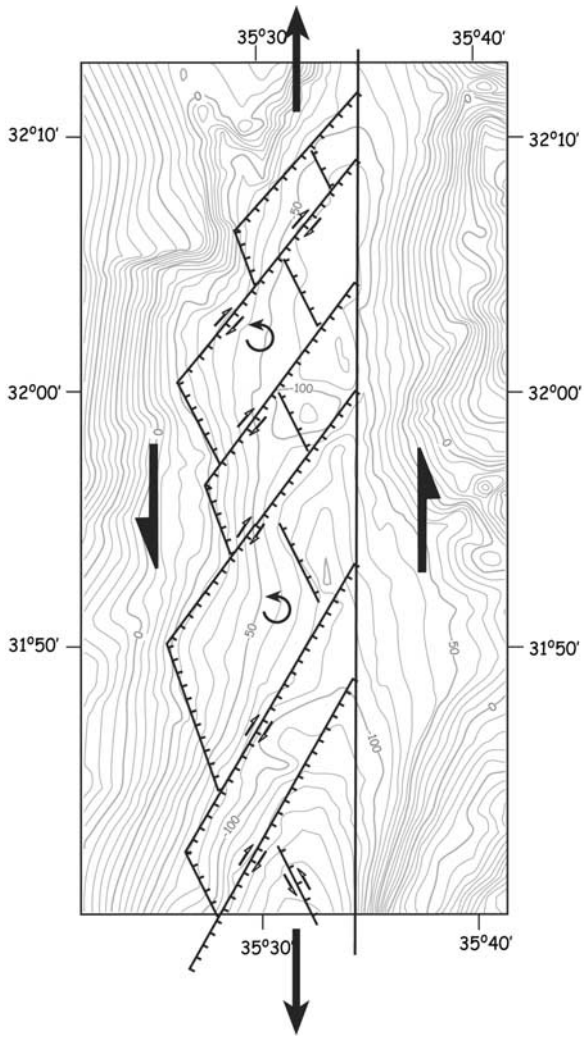

Figure 12. Schematic block model of the Dead Sea Transform in the Jericho Valley, superposed on the gravity (Bouguer) anomaly map [*ten Brink et al.*, 1993].

[35] One expected consequence of the proposed mechanism is the appearance of mixed earthquake mechanisms in the deforming zone: Dextral motion along NW-NNW and NNE-NE faults due to counterclockwise rotation, and sinistral motion along the boundaries of the shear zone. This is apparently consistent with the observed fault plane solutions (Figure 9) and with observations of both dextral and sinistral slip indications along the western

boundary of the Dead Sea basin [e.g., *Agnon*, 1983].

[36] As mentioned above, both experimental [*Bartlett et al.*, 1981; *Freund*, 1974; *Schreurs*, 1994; *Beeler et al.*, 1996] and analytic [*Braun*, 1994; *Morgan and Boettcher*, 1999; *Aharonov and Sparks*, 2002] studies have the general result that a dominant mode of shear deformation in newly formed strike slip zones are oblique ("Riedel") shears. These evolve with progressive strain and delimit local domains that rotate about vertical axes, as expected on theoretical grounds [*McKenzie and Jackson*, 1983]. In left lateral strike slip zones, such fractures are oriented counterclockwise relative to the shear zone direction, while in the Jericho Valley the NNE-trending fault system is oriented clockwise with respect to the transform direction. This would imply that the internal fault systems in the Jericho Valley predated and were reactivated by the sinistral motion along the Dead Sea Transform.

[37] It is not yet known how the upper crustal block structure is decoupled from the plate boundary shear zone in the lower crust and upper mantle. Seismic reflection lines in this area penetrate only about 3 s TWTT, i.e., 3–4 km at the most, which is insufficient to detect possible deep crustal, low-angle decoupling detachments, as observed in the San Andreas–San Jacinto fault system [*Nicholson et al.*, 1986].

5. Conclusions

[38] 1. Integration of seismic reflection, seismological and structural data suggests that shear in the Jericho Valley section of the Dead Sea Transform evolved from a localized strike slip to a broad, distributed fault system. This change was presumably associated with the change in the relative Africa/Arabia Euler vector in the Pliocene.

[39] 2. The major DST segment in the early phase was the Jericho fault, which formed the western boundary of a narrow basin, presumably a pull-apart, bounded on the east by the DST eastern boundary fault. This basin is a northward extension of the northern Dead Sea basin. It apparently extends now to a depth of at least 2.5–3.0 km and is filled primarily by Neogene-Pliocene, fluvial-clastic deposits that flowed energetically into the basin as well as evaporites.

[40] 3. A tectonic and depositional change, presumably associated with the Pliocene onset of transtension across the DST, resulted in cessation of shear along the N-S striking Jericho fault and appearance of a penetrative deformation field that prevailed over a much broader shear zone. It has been characterized by a bimodal distribution (NW-NNW and NNE-NE) of fault systems, post-Pleistocene fracture sets and recent earthquake mechanisms.

[41] 4. Early-phase salt has apparently utilized the Jericho fault zone as a conduit for diapirism. This caused the uplift, passive collapse (normal faulting) and tilting of Late Pleistocene and Holocene sediments currently observed along the ~15 km long Jericho Lineament but disappearing southward toward the Dead Sea basin. These salt-induced surface features generally trace the early-phase Jericho fault but do not express its current activity, certainly not as a major strand of the DST

[42] 5. In the late phase, fine, low-energy fluvial and lacustrine deposits filled a broad basin, overlying the Jericho fault and the early-phase inner basin. The late-phase basin was created by eastward down-faulting across NNE and NW trending faults, while the major subsidence has taken place closer to the eastern boundary fault.

[43] 6. Although poorly clustered, current microseismicity shows that the Pliocene to Recent tectonic regime involves dextral-normal motion on NNE-NE striking faults confined to the transform basin (e.g., Nuweime fault). The Kalia fault, forming a prominent bathymetric scarp in the northwestern Dead Sea basin, is part of this system and a preferred candidate for the destructive 1927 Jericho earthquake, although its continuation to the eastern part of the basin is currently unresolved.

[44] 7. Both localized/segmented and distributed shear is currently observed along all major continental transform plate boundaries, as well as at smaller scales. The delocalized structure of the DST in the Jericho Valley is apparently a dilational version of the "bookshelf" mechanism, in which the sinistral plate motion is accommodated by counterclockwise rotation of an array of internal fault sets. As yet, there is no paleomagnetic confirmation for this rotation and no observations pertinent to the decoupling between the upper and lower crust.

Acknowledgments

[45] We are grateful to J. Beavan and an anonymous reviewer for thoughtful reviews, to U. ten Brink, S. Belitzky, M. Gardosh, L. Fleischer, H. Ron, U. Frieslander, and

G. Baer for helpful discussions, to M. Elimelekh, B. Medvedev, and Y. Sagi for seismic data processing, to A. Almogi for paleontological analysis, to Z. Garfunkel and S. Marco for sharing field observations, and to R. Gafsu for technical support. Z. Garfunkel and B. Z. Begin are thanked for commenting on an early version of this manuscript. Data processing and analysis were funded by the U.S.-Israel Bi-National Fund, grant 97-00286/1.

References

Abelson, M., G. Baer, V. Shtivelman, D. Wachs, E. Raz, O. Crouvi, I. Kurzon, and Y. Yechieli (2003), Collapse-sinkholes and radar interferometry reveal neotectonics concealed within the Dead Sea basin, *Geophys. Res. Lett.*, *30*(10), 1545, doi:10.1029/2003GL017103.

Agnon, A. (1983), Evolution of sedimentary basins and morphotectonics in the south-western boundary fault system of the Dead Sea, M.Sc. thesis, Hebrew Univ., Jerusalem.

Aharonov, E., and D. Sparks (2002), Shear profiles and localization in simulations of granular material, *Phys. Rev. E*, *65* article 051302, doi:10.1103/PhysRevE.65.051302.

Al-Zoubi, A., and U. S. ten Brink (2001), Salt diapirs in the Dead Sea basin and their relationship to Quaternary extensional tectonics, *Mar. Pet. Geol.*, *18*, 779–797.

Bartlett, W. L., M. Friedman, and J. M. Logan (1981), Experimental folding and faulting of rocks under confining pressure. Part IX. Wrench faults in limestone layers, *Tectonophysics*, *79*, 255–277.

Beeler, N. M., T. E. Tullis, M. L. Blanpied, and J. D. Weeks (1996), Frictional behavior of large displacement on experimental faults, *J. Geophys. Res.*, *101*, 8697–8715.

Begin, Z. B. (1973), The geological map of Israel (1:50, 000), Jericho sheet, Geol. Surv. of Isr., Jerusalem.

Belitzky, S. (1996), Tectonic geomorphology of the lower Jordan Valley-An active continental rift (in Hebrew, with extended English abstract), Ph.D. thesis, Hebrew Univ. of Jerusalem.

Belitzky, S., and Y. Mimran (1996), Active salt diapirism at the Zahrat El-Qurein dome, lower Jordan Valley (Jordan), *Isr. J. Earth Sci.*, *45*, 11–18.

Ben-Avraham, Z. (1985), Structural framework of the Gulf of Elat (Aqaba)-northern Red Sea, *J. Geophys. Res.*, *90*, 703–726.

Bender, F. (1968), *Geologie von Jordanien*, Begruder Borntraeger, Berlin.

Bentor, Y. K., and A. Vroman (1960), The geological map of Israel, scale 1:100.000, sheet 16, Mt Sedom, 2nd edition, with explanatory notes, 117 pp., Govt. Printer, Jerusalem.

Braun, J. (1994), Three-dimensional numerical simulations of crustal-scale wrenching using a non-linear failure criterion, *J. Struct. Geol.*, *8*, 1173–1186.

Enzel, Y., G. Cadan, and Y. Eyal (2000), Holocene earthquakes in the Dead Sea graben from a fan-delta sequence, *Quat. Res.*, *53*, 34–48.

Eyal, M., Y. Eyal, Y. Bartov, and G. Steinitz (1981), The tectonic development of the western margin of the Gulf of Elat (Aqaba) Rift, *Tectonophysics*, *80*, 39–66.

Ezersky, M. (2003), Study of the shallow subsurface sinkhole hazard areas along the Dead Sea shore using geophysical methods, *Rep. 211/247/02*, Geophys. Inst. of Isr., Lod, Israel.

Feigin, G., and A. Shapira (1994), A unified crustal model for calculating travel times of seismic waves across the Israel seismic network, *Rep. Z1/567/79(107)*, Geophys. Inst. of Isr., Lod, Israel.

Freund, R. (1965), A model of the structural development of Israel and adjacent areas since the Upper Cretaceous times, *Geol. Mag.*, *102*, 189–205.

Freund, R. (1974), Kinematics of transform and transcurrent faults, *Tectonophysics*, *21*, 93–134.

Gardosh, M. (1987), The stratigraphy and tectonic evolution of Quaternary sediments in the Dead Sea region (Hebrew with English abstract), M.Sc. thesis, Hebrew Univ. of Jerusalem.

Gardosh, M., Z. Reches, and Z. Garfunkel (1990), Holocene tectonic deformation along the western margins of the Dead Sea, *Tectonophysics*, *180*, 123–137.

Gardosh, M., E. Kashai, S. Salhov, H. Shulman, and E. Tennenbaum (1997), Hydrocarbon exploration in the southern Dead Sea basin, in *The Dead Sea: The Lake and Its Setting*, edited by T. M. Niemi, Z. Ben Avraham, and J. R. Gat, pp. 57–72, Oxford Univ. Press, New York.

Garfunkel, Z. (1981), Internal structure of the Dead Sea leaky transform (rift) in relation to plate kinematics, *Tectonophysics*, *80*, 81–108.

Geophysical Institute of Israel (2004), The earthquakes catalog of Israel and its surroundings, 1907–2004, Jerusalem.

Hall, J. K. (1993), The GSI digital terrain model (DTM) project completed, *Geol. Surv. Isr. Current Res.*, *8*, 47–50.

Heimann, A., and H. Ron (1993), Geometric changes of plate boundaries along part of the northern Dead Sea transform: Geochronologic and paleomagnetic evidence, *Tectonics*, *12*, 477–491.

Joffe, S., and Z. Garfunkel (1987), Plate kinematics of the circum Red Sea-A re-evaluation, *Tectonophysics*, *141*, 5–22.

Kashai, E. L., and P. F. Croker (1987), Structural geometry and evolution of the Dead Sea-Jordan rift system as deduced from new subsurface data, *Tectonophysics*, *141*, 33–60.

Lamb, S. H., and H. M. Bibby (1989), The last 25Ma of rotational deformation in part of the New Zealand plate boundary zone, *J. Struct. Geol.*, *11*, 473–492.

Mandl, G. (1987), Tectonic deformation by rotating parallel faults: The "bookshelf" mechanism, *Tectonophysics*, *141*, 277–316.

McKenzie, D. P., and J. Jackson (1983), The relationship between strain rates, crustal thickening, paleomagnetism, finite strain and fault movements within a deforming zone, *Earth Planet. Sci. Lett.*, *65*, 182–202.

Miller, D. D. (1998), Distributed shear, rotation and partitioned strain along the San Andreas Fault, central California, *Geology*, *26*, 867–870.

Morgan, J. K., and M. S. Boettcher (1999), Numerical simulations of granular shear zones using the distinct element method: 1. Shear zone kinematics and micromechanics of localization, *J. Geophys. Res.*, *104*, 2703–2719.

Natural Resources Authority (2004), Earthquakes in Jordan and adjacent areas, 1984-2004, Seismol. Div., Jordan Seismol. Obs., Amman, Jordan.

Neev, D., and K. O. Emery (1967), The Dead Sea: Depositional processes and environments of evaporites, *Bull. Geol. Surv. Isr.*, *41*, 1–147.

Neev, D., and J. K. Hall (1979), Geophysical investigation of the Dead Sea, *Sediment. Geol.*, *23*, 209–238.

Nicholson, C., L. Seeber, P. Williams, and L. Sykes (1986), Seismicity and fault kinematics through the Eastern Transverse ranges, California: Block rotation, strike slip faulting and low angle thrusts, *J. Geophys. Res.*, *91*, 4891–4908.

Picard, L. (1943), Structure and evolution of Palestine (with comparative notes on neighboring countries), *Bull. Geol. Dept. Hebrew Univ.*, *4*, 1–187.

Quennell, A. M. (1956), Geological map of Jordan east of the Rift Valley, 1:250,000, Dept. of Lands and Surv. of Jordan, Govt. of the Hashemite Kingdom of Jordan.

Quennell, A. M. (1959), The structural and geomorphic evolution of the Dead Sea Rift, *Q. J. Geol. Soc. London*, *114*, 1–24.

Reasenberg, P. A., and D. Oppenheimer (1985), FPFIT, FPPLOT and FPPAGE: Fortran computer programs for calculating and displaying earthquake fault-plane solutions, *U.S. Geol. Surv. Open File Rep.*, *85-739*.

Reches, Z., and D. F. Hoexter (1981), Holocene seismic and tectonic activity in the Dead Sea area, *Tectonophysics*, *80*, 235–254.

Reilinger, R., N. Toksoz, S. McClusky, and A. Barka (2000), 1999 Izmit, Turkey Earthquake Was No Surprise, *GSA Today*, *10*(1), 1–6.

Roberts, A. P. (1995), Tectonic rotation about the termination of a major strike slip fault, Marlborough fault system, New Zealand, *Geophys. Res. Lett.*, *22*, 187–190.

Rotstein, Y., Y. Bartov, and A. Hofstetter (1991), Active compressional tectonics in the Jericho area, Dead Sea Rift, *Tectonophysics*, *198*, 239–259.

Sagi, A. (1999), Jointing and faulting processes along the western margins of the Dead Sea basin (Hebrew with English abstract), M.Sc. thesis, Hebrew Univ. of Jerusalem.

Schreurs, G. (1994), Experiments on strike-slip faulting and block rotation, *Geology*, *22*, 567–570.

Shamir, G., I. Bruner, Y. Eyal, and L. Fleischer (2002), High-resolution structure of the Dead Sea transform in the northern Dead Sea basin, paper presented at Annual Conference of the Israel Geological Society, Ma'agan, Israel.

Shapira, A. (1988), Magnitude scales for regional earthquakes monitored in Israel, *Isr. J. Earth Sci.*, *37*, 17–22.

Shapira, A., R. Avni, and A. Nur (1992), A new estimate for the epicenter of the Jericho earthquake of 11 July 1927, *Isr. J. Earth Sci.*, *42*, 93–96.

Shertok, E. Z. (1980), Jericho-1: Geological completion report, *Rep. 80/21*, Oil Explor. (Investments) Ltd., Tel Aviv, Israel.

Stevens, C. W., R. McCaffrey, Y. Bock, J. F. Genrich, M. Pubellier, and C. Subarya (2002), Evidence for block rotations and basal shear in the world's fastest slipping continental shear zone in NW New Guinea, in *Plate Boundary Zones*, *Geodyn. Ser.*, vol. 30, edited by S. Stein and J. T. Freymueller, pp. 87–99, AGU, Washington, D. C.

ten Brink, U. S., Z. Ben Avraham, R. E. Bell, M. Hasounneh, D. F. Coleman, G. Andreasen, G. Tibor, and B. Coakley (1993), Structure of the Dead Sea pull-apart basin from gravity analyses, *J. Geophys. Res.*, *98*, 21,877–21,894.

ten Brink, U. S., M. Rybakov, A. S. Al-Zoubi, M. Hasounneh, U. Frieslander, A. Batayneh, V. Goldschmidt, M. N. Daoud, Y. Rotstein, and J. K. Hall (1999), Anatomy of the Dead Sea transform: Does it reflect continuous changes in plate motion?, *Geology*, *27*, 887–890.

Trusheim, F. (1960), Mechanism of salt migration in northern Germany, *Am. Assoc. Pet. Geol. Bull.*, *44*, 1519–1540.

Vendeville, B. C., and M. P. A. Jackson (1992), The rise of diapers during thin-skinned extension, *Mar. Pet. Geol.*, *9*, 331–353.

Waldhauser, F., and W. Ellsworth (2000), A double-difference earthquake location algorithm: Method and application to the Northern Hayward Fault, California, *Bull. Seismol. Soc. Am.*, *90*, 1353–1368.

Wallace, R. E. (1990), The San Andreas Fault System, California, *U.S. Geol. Surv. Prof. Pap.*, *1515*.

Yilmaz, O. (2001), *Seismic Data Analysis: Processing, Inversion, and Interpretation of Seismic Data*, Soc. Explor. Geophys., Tulsa, Okla.

Zak, I. (1967), The geology of Mt. Sedom (in Hebrew with English abstract), Ph.D. thesis, Hebrew Univ. of Jerusalem.

Zak, I., and R. Freund (1981), Asymmetry and basin migration in the Dead Sea rift, *Tectonophysics*, *80*, 27–38.